



Research Paper

Composite Palladium Alloy Membranes for Separation and Recovery of Hydrogen in Bio-jet Fuel Production Unit

Ritu Parashar^{1,2}, Bipin Chandra Nailwal², Nitesh Goswami², Raja Kishora Lenka³, Soumitra Kar^{1,2,*}, Asis Kumar Adak², Anil Kumar Sinha⁴, Suresh Chandra Parida^{1,5}, Sulekha Mukhopadhyay^{1,6}

¹ Homi Bhabha National Institute, Anushaktinagar, Mumbai - 400094, India

² Desalination & Membrane Technology Division, Bhabha Atomic Research Centre, Trombay, Mumbai - 400085, India

³ Powder Metallurgy Division, Materials Group, Bhabha Atomic Research Centre, Vashi Complex, Navi Mumbai - 400705, India

⁴ CSIR-Indian Institute of Petroleum, Dehradun - 248005, India

⁵ Product Development Division, Bhabha Atomic Research Centre, Trombay, Mumbai - 400085, India

⁶ Chemical Engineering Division, Bhabha Atomic Research Centre, Trombay, Mumbai - 400085, India

Article info

Received 2022-05-20

Revised 2022-09-02

Accepted 2022-09-16

Available online 2022-09-16

Keywords

Bio-jet fuel

Composite metal membrane

Hydrogen

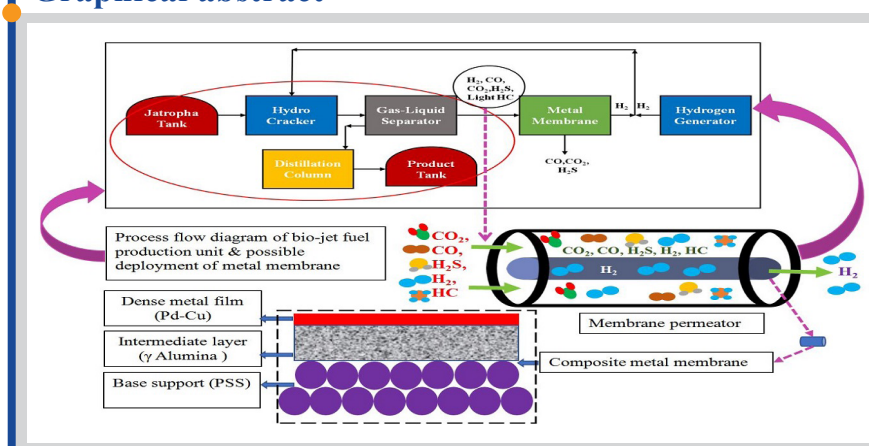
Palladium alloy

Magnetron Sputtering

Highlights

- Characterization and gas permeation studies of porous stainless-steel (PSS) support.
- Parametric optimization for coating of the intermediate layer of alumina on PSS.
- Fabrication and characterization of alumina-coated PSS composite support.
- Pd-Cu alloy composite metal membrane fabricated and characterized.
- Gas permeation, stability, and compatibility studies of Pd-Cu alloy membrane in a bio-jet fuel production environment.
- Studies on regeneration of membrane.

Graphical abstract



Abstract

Hydro-processing is a crucial step in bio-jet fuel production. The left-over hydrogen in the vent gas from the hydrocracker cannot be recycled back as it contains several impurities like light hydrocarbons & H_2S . Here we report the development of composite palladium alloy membranes for the recovery of hydrogen from the simulated bio-jet fuel production environment, which is investigated for the first time. The metal membranes were fabricated on porous stainless steel (PSS) tubes as support. An intermediate alumina layer was coated over support using vacuum-assisted dip coating. The He/Ar gas selectivity of composite support was determined to be 4.92 at 0.05 bar (trans-membrane pressure). A dense thin film (~4 μm) of Pd (60 wt.%) - Cu (40 wt.%) metal was coated on composite support by the DC magnetron sputter deposition technique. The membrane was tested in simulated gas having the composition of vent gas stream of hydrocracker, as a preparatory step before application in the actual environment. The permeance of the in-house developed membrane was found to be ~1 GPU with a hydrogen recovery of 37 and 54% at 1.5 bar and 2 bar, respectively. The membrane permeance after exposure to a vent gas environment for 24 hours was reduced by ~75%. The membrane was regenerated in a mixture of H_2 (10%) - He (90%) at 0.2 bar and 250 °C for 5 hours, and the flux was restored up to 85% of the flux of the unexposed membrane. The studies have opened up a new domain of application for metal membranes.

© 2022 FIMTEC & MPRL. All rights reserved.

1. Introduction

It is important to search for renewable fuels for the sustainable development of mankind. ~781 Mt of CO_2 is emitted from air transport, which

is > 2% of CO_2 emissions due to human activities [1,2]. Bio-jet fuel derived from sustainable plant products is an important step toward carbon-neutral fuel

* Corresponding author: soubiswa@barc.gov.in (S. Kar)

that can reduce global warming issues and the associated challenges arising from climate change. Also, bio-jet fuel reduces dependency on fossil-based sources while reducing carbon footprints by ~ 80% [3]. The first-generation biofuel is mainly produced from grains, sugar, or seeds. Second-generation biofuel is produced from non-edible crops like jatropha [4–6]. Biological, physico-chemical, and thermo-chemical methods are used for the production of biofuels from biomass [7–11]. Hydro-processing is an important process in bio-jet fuel production in which hydrogen is used as a reactant in excess [12,13]. Vent gas having ~ 80% of hydrogen from the hydrocracker cannot be recycled back as it contains several impurities like H₂S and light hydrocarbons that poison the catalyst in the hydrocracker unit. The hydrogen present in the vent stream can be recovered for recycling and reuse, as shown in Fig. 1. This will reduce the load on the hydrogen generation unit significantly, making the overall process more economic. The existing bio-jet fuel production process is shown in the encircled portion of Fig. 1, where excess hydrogen is vented into the atmosphere in the present arrangement.

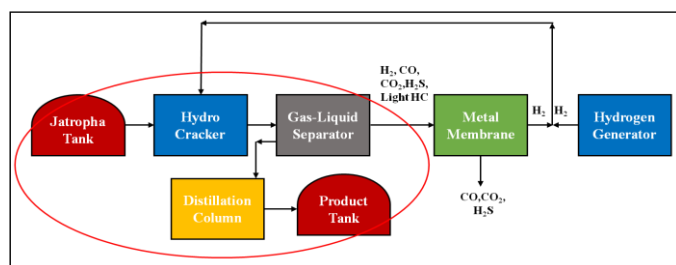


Fig. 1. Process flow diagram of bio-jet fuel production unit & possible deployment of the metal membrane.

Metal membrane-based separation process [14–17] can be potentially used for the separation and recovery of hydrogen [18]. Unlike typical large-scale hydrocrackers, where pressure swing adsorption (PSA) technology is used for hydrogen purification, bio-jet fuel production plants are expected to be of a smaller scale due to feedstock availability issues. Hence, small modular purification systems based on membrane technology are a suitable option. Solution diffusion is the predominant mechanism of hydrogen transport in a metal membrane. It is a multi-step process involving the transportation of molecules to the membrane surface, dissociative adsorption on the active surface, transfer from the surface to the interstitial bulk site, diffusion of hydrogen atoms, transfer of atoms from the solution to the permeate side, and associative desorption of molecule from the surface [19]. Owing to the solution diffusion mechanism, only hydrogen gas is transported, excluding all other gases.

Composite metal membranes are generally used for hydrogen separation, instead of pure metal tubes, in view of having higher throughput at a lower cost [20]. For high-pressure applications, porous membrane supports like stainless steel, Hastelloy, and nickel are generally used due to their higher mechanical strength and better leak-tight configurations compared to ceramics and glass. Their thermal expansion coefficients are also similar to the metals of interest which are used for hydrogen separation, such as palladium [21–23]. The commercially available porous supports have large pore sizes with a wide distribution of pore sizes and high surface roughness [24,25] which is not desirable. Hence, the porous metallic support can be coated with an intermediate ceramic layer to improve the substrate's surface characteristics, reduce the pore size and avoid inter-metallic diffusion (between the porous metal layer and metal membrane). Therefore, in many cases, ceramic materials like TiO₂, ZrO₂, SiO₂, Al₂O₃, etc. are used as an intermediate layer over highly porous metal [26,27] to form composite support. Various ceramic coating techniques are available such as hydrothermal synthesis, plasma spraying, solid-state sintering, and sol-gel coating [28,29]. Subsequently, the composite support can be coated with the metal of interest by DC magnetron sputtering, which offers advantages of high deposition rate, ease of operation, high purity films, high adherence, and excellent uniformity [30–32].

The literature reports abundant evidence that the Pd-Cu membrane is an excellent candidate for hydrogen separation in comparison with Pd and other Pd alloys [33–36]. The maximum hydrogen permeability for Pd-Cu alloys is reported at 40 wt.% Cu [i.e., Pd (60 wt.%) - Cu (40 wt.%)], because of the formation of a body-centered cubic (bcc) crystal lattice. The membrane cost is also significantly decreased due to the high percentage of Cu [33,35,37,38]. In addition, Pd-Cu alloys have high hydrogen selectivity, thermal stability, and resistance against poisoning with stability over a wide operating temperature range [25,39,40]. It has been reported [14] that the Pd-Cu membrane showed

stable performance with respect to hydrogen permeation flux for exposure to 5–39 ppm of H₂S for 618 hours. Another study [38] has been reported investigating the effect of H₂S on the hydrogen permeance of Pd-Cu alloy membranes, which were exposed to a 1000 ppm H₂S gas in a temperature range of 603 to 1123 K and 620 kPa pressure. The studies confirmed that there was no deterioration in the hydrogen permeance of Pd (80% wt.) - Cu (20% wt.) alloy membrane over the entire temperature range in an H₂S environment [38]. There is ample evidence available in the literature that Pd-Cu alloy is resistant to sulfur poisoning with H₂S concentrations up to 5 ppm [38,41], 50 ppm [36], 1000 ppm [38,42], and 100,000 ppm [38,43]. Several studies reported that in addition to H₂S, CO and CO₂ also have an adverse effect on Pd and Pd alloy membranes. The hydrogen permeance is reduced due to the adsorption of CO and CO₂ on the surface which blocks hydrogen adsorption sites and reduces the active area of H₂ for the dissociation of H₂ molecules, causing “blanketing” effects [34,44,45]. Another reason for the reduction of hydrogen permeability is the coking effect on the membrane surface. The presence of carbon-containing gases results in carbon deposition on the active surface and resultant deactivation of the surface sites which leads to a reduction in hydrogen permeability [34,44,46,47].

In this work, a composite Pd-Cu alloy metal membrane was developed and tested for recovery of hydrogen from the simulated vent stream of the bio-jet fuel production unit, which is investigated for the first time. This work includes the characterization of porous stainless steel (PSS), its surface modification by coating with an intermediate layer of alumina using vacuum-assisted dip coating, subsequent coating of composite support with Pd-Cu alloy using DC magnetron sputtering, along with performance evaluation of the in-house developed membranes in simulated bio-jet fuel environment and membrane regeneration studies.

2. Materials and Methods

2.1 Fabrication of ceramic coated PSS membrane support

The PSS support tubes were procured from M/s Diva Envitech, India. The characterization of the support tube was carried out using scanning electron microscopy (SEM, Oxford Instrument, Zeiss Evo 18) and gas permeation studies. Argon and helium were used for room temperature gas permeation studies of PSS support. Alumina powder was used for the fabrication of an intermediate ceramic layer over the base PSS support. The powder was characterized by Brunauer–Emmett–Teller (BET) surface area analyzer (Sorptomatic), X-ray diffraction (INEL), and dilatometer (SETARAM Instruments, Model Setsys Evolution 1750). The ceramic slurry was prepared in a 1:1 mixture of methyl ethyl ketone (MEK) and ethanol. Oleic acid was used as a dispersant and polyvinyl butyral (4% PVB) was used as a pore former. Dioctyl Phthalate (DOP) was used as a plasticizer and PEG-400 as the binder. The slurry was prepared by mixing alumina powder, solvent, and dispersant for 72 hours in a ball mill followed by further mixing of other chemicals (binder and pore former) for 24 hours. The chemicals required for this process were procured from SRL, India. The slurries were labeled as Slurry 1 to 4 for alumina loadings varying from 5 to 20% with an increment of 5% in each sample. Subsequently, ceramic coating over PSS support was carried out for 30 seconds at a vacuum of 100 torrs by dip coating (with a withdrawal speed of 5 mm/s and a dipping duration of 10 s). Sintering of coated samples was carried out in air followed by a nitrogen environment as per the profile shown in Table 1. The heating was done at a temperature of 300 °C in the air to allow the organics and volatile components to oxidize and escape as vapors. Subsequently, heating was done up to 700 °C in a nitrogen environment. This temperature was optimized based on the dilatometry analysis. Adhesion test analyses of the sintered coated samples were also carried out with the help of an ultrasonic instrument (SONIX IV). For this, the sample was dipped in ethanol and ultrasonicated. The weight of the sample was measured every 15 minutes until a constant weight was observed.

2.2 Metal coating on ceramic coated PSS

Fig. 2 shows the DC magnetron sputtering assembly, which was used for coating a thin layer of Pd-Cu alloy on the PSS-alumina composite support (length: 500 mm, outer diameter: 12 mm). The metal alloy was coated on composite support at the following optimum set of operating conditions; deposition pressure: 8.5 mtorr, at a power of 0.2 kW, and gas flow rate: 60 standard cubic centimeters per minute. Vacuum annealing of the metal-coated tube was carried out in a vacuum furnace (Hind Hivac, India) at a vacuum of 5 × 10⁻⁵ torr in an argon atmosphere at 450 °C.

Table 1
Sintering profile for alumina coated PSS sample.

S. No.	Sequence	Gas used	T1 (°C)	T2 (°C)	Rate of heating (°C/min)	Period (hours)
1	Heat	Air	Ambient	300	0.5	-
2	Dwell	Air	300	300	-	2
3	Heat	Nitrogen	300	700	1	-
4	Dwell	Nitrogen	700	700	-	3
5	Cool	Nitrogen	700	Ambient	1	-

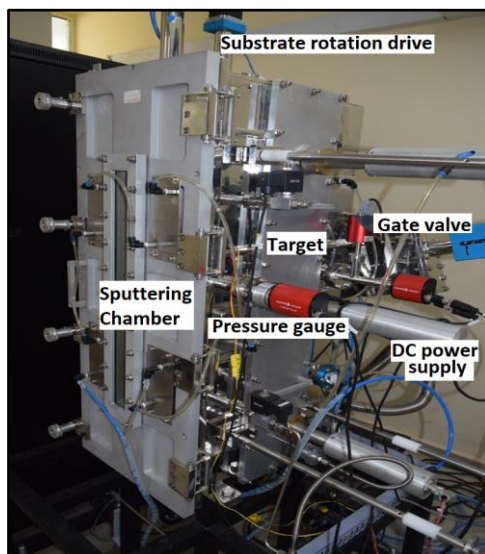


Fig. 2. DC Magnetron sputtering assembly.

2.3 Gas Permeation studies

Fig. 3 shows the membrane permeator. It consists of an outer shell, support tube, graphite gasket, graphite ferrules, metal membrane, and end connectors. The outer shell and support tube were made of SS-316. The membrane was sealed with end connectors using graphite ferrules.

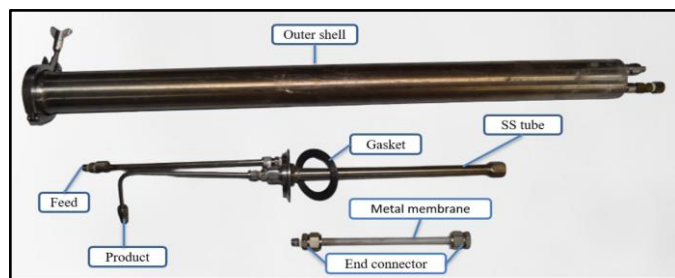


Fig. 3. Membrane permeator showing the individual components.

2.4 Hydrogen separation studies in the simulated environment

Fig. 4 shows the schematic of the setup used for testing of Pd-Cu membrane in a simulated vent gas stream of a bio-jet fuel production unit (carbon monoxide 1.5, carbon dioxide 1.5, methane 6.5, ethane 5, propane 2, n-Butane 1, iso-Butane 1, n-Pentane 0.25, iso-Pentane 0.25, hydrogen sulfide 1 & hydrogen 80%). The helium leak rate of the membrane permeator was found to be 4×10^{-4} mbar.L/s. The composition of the reject stream was measured using Quadrupole Mass Spectrometer (QMS; Hiden Analytical).

2.5 Membrane permeance calculation

The hydrogen permeance (ϕ) was calculated using Equation 1 known as Sievert's law [39]:

$$J = \phi \times \Delta P^n \tag{1}$$

Where J is the flux of membrane in $\text{mol. m}^{-2} \text{ h}^{-1}$, ϕ is permeance in $\text{mol. m}^{-2} \text{ h}^{-1} \text{ Pa}^n$, ΔP is trans-membrane pressure in Pa and n is an exponent which depends on the rate controlling step. As the thickness of the Pd-Cu metal membrane is very less ($\sim 4 \mu\text{m}$), the mass transfer controlling step has been considered to be the hydrogen adsorption and desorption on metal for which $n \sim 1$ [25].

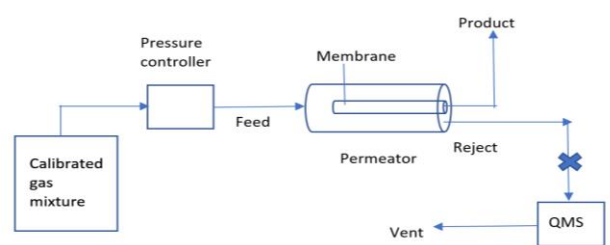


Fig. 4. Schematic of setup used for gas permeation studies of Pd-Cu membrane.

3. Results and Discussion

3.1 Characterization of PSS support

Fig. 5 shows the SEM image of PSS support. It is clear from the SEM image that the support has most of the pores in the 5 - 10 μm range, while some defects are of higher size ($\sim 20 \mu\text{m}$), as shown in the red encircled zones in the SEM image. The image confirms that the PSS support has a good pore density with interconnected pores.

Fig. 6 shows the Hg porosimetry analysis of PSS support. It shows that the pore size of the support is $\sim 7.05 \mu\text{m}$ with a porosity of $\sim 20\%$. It was found that $\sim 70\%$ of the pores are in the size range of 6 - 7.5 μm and $\sim 10\%$ of the pores are of sub-micron size (0.1 - 1 μm). The total pore volume was found to be $\sim 34 \text{ mm}^3/\text{g}$.

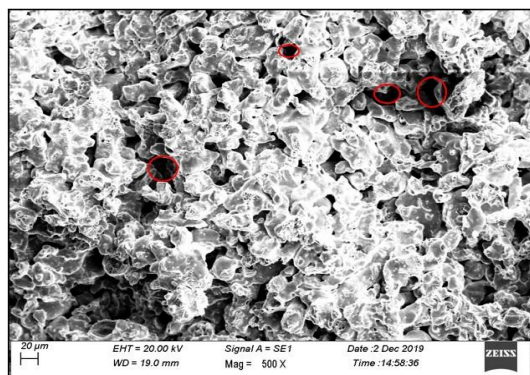


Fig. 5. Surface morphology of PSS support.

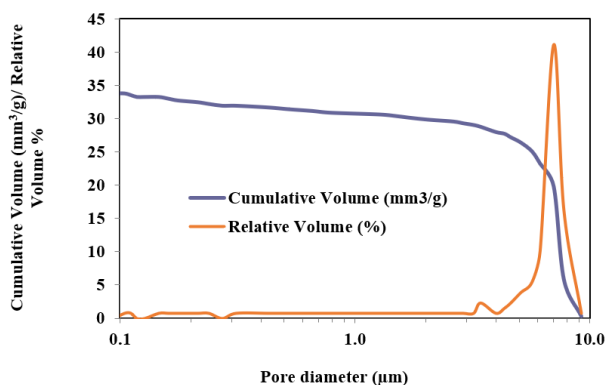
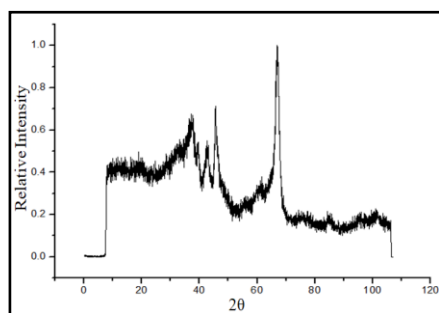


Fig. 6. Porometry analysis of PSS support.

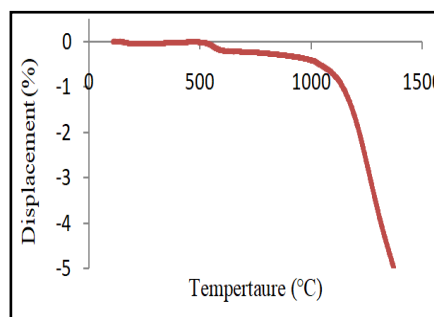
Gas permeation studies of PSS support were carried out with helium and argon at 0.05 bar and 0.1 bar in the dead-end mode of operation at ambient temperature. Feed was introduced in the annular zone of the permeator and the product was taken out from the tube side. Table 2 shows the flux and selectivity of the PSS support. It was observed that with an increase in pressure from 0.05 to 0.1 bar, the flux of helium, as well as argon through the PSS tube, becomes almost twice and selectivity remains nearly constant in the range of 1.8-1.9.

Table 2
Gas permeation studies of PSS support.

Pressure (bar)	Flux (mol.m ⁻² .h ⁻¹)		Permeance (mol.m ⁻² .h ⁻¹ .Pa ⁻¹)		Gas selectivity (He/Ar)
	He	Ar	He	Ar	
0.05	125.90 ± 46	64.46 ± 18	0.0252	0.0128	1.9
0.1	251.81 ± 94	137.08 ± 34	0.0252	0.0137	1.8



(a) XRD pattern of alumina powder.



(b) Dilatometry studies of alumina.

Fig.7. Characterization of alumina powder.

This also confirms the flow domain to be in the mixed-flow regime [48]. This is attributed to the effect of gas diffusion through the pores of sub-micron size.

3.2 Characterization of alumina powder

The specific surface area of alumina, as determined using the BET technique was found to be 62.095 m²/g using BET technique and the particle size was ~ 26 nm. The density of powder was considered to be 3.987 g/cc [49].

Fig. 6 (a) shows the XRD pattern of alumina. The peaks at 2θ values of 37°, 42°, and 67° correspond to the α-phase and 39° to γ-phase of alumina [50]. It shows that the powder is a mixture of α- and γ- phases of alumina.

Fig. 7 (b) shows the dilatometry plot of alumina powder, which confirms that the sintering of alumina powder starts beyond 600 °C. The final sintering temperature was fixed at 700 °C in order to ensure that the sintering of alumina particles leads to the coating of the alumina layer over PSS support.

3.3 Characterization of PSS-alumina composite support

Table 3 shows the adhesion test results of alumina-coated PSS, as calculated by Equation 2. It can be observed that the adhesion of the sample increases from 0.4 to 1.8% (Slurry 1 to 3) with an increase in solid loading from 5 to 15%, which increases the viscosity of the solution. Beyond 15% solid loading (Slurry 4 at 20% loading), the extent of adhesion becomes nearly constant at 1.8%. Therefore, Slurry 3 was chosen as the optimum.

$$\text{Adhesion (\%)} = \frac{W_{\text{final}} - W_{\text{initial}}}{W_{\text{initial}}} \times 100 \quad (2)$$

Fig. 8(a-d) shows the SEM images of alumina-coated PSS support with different solid loadings. In the case of Slurry 1 with 5% solid loading (Fig. 8(a)), some cracks and pits were observed, indicating non-uniform coating. In the case of Slurry 2 with 10% solid loading (Fig. 8(b)), some agglomerated patches were observed, indicative of non-uniform coating. In the case of Slurry 3 with 15% solid loading (Fig. 8(c)), a continuous coating with nano-pores was observed, although some defects of ~ 2 μm size were also observed. In the case of Slurry 4 with 20% solid loading (Fig. 8(d)), a dense coating was obtained over the base support, as compared to other coated samples. Thus, 15% solid loading (Slurry 3) was chosen as the optimum.

Table 4 shows the He/Ar gas permselectivity of alumina-coated PSS support. The permselectivity increased in comparison to the bare PSS tube from 1.8 to 4.06 (at 0.1 bar pressure) and from 1.9 to 4.92 (at 0.05 bar pressure), which is due to the decrease in the pore size by alumina coating. With the decrease in pressure, the selectivity was found to increase due to the shift of the flow domain from viscous flow to the Knudsen diffusion regime [48].

Table 3

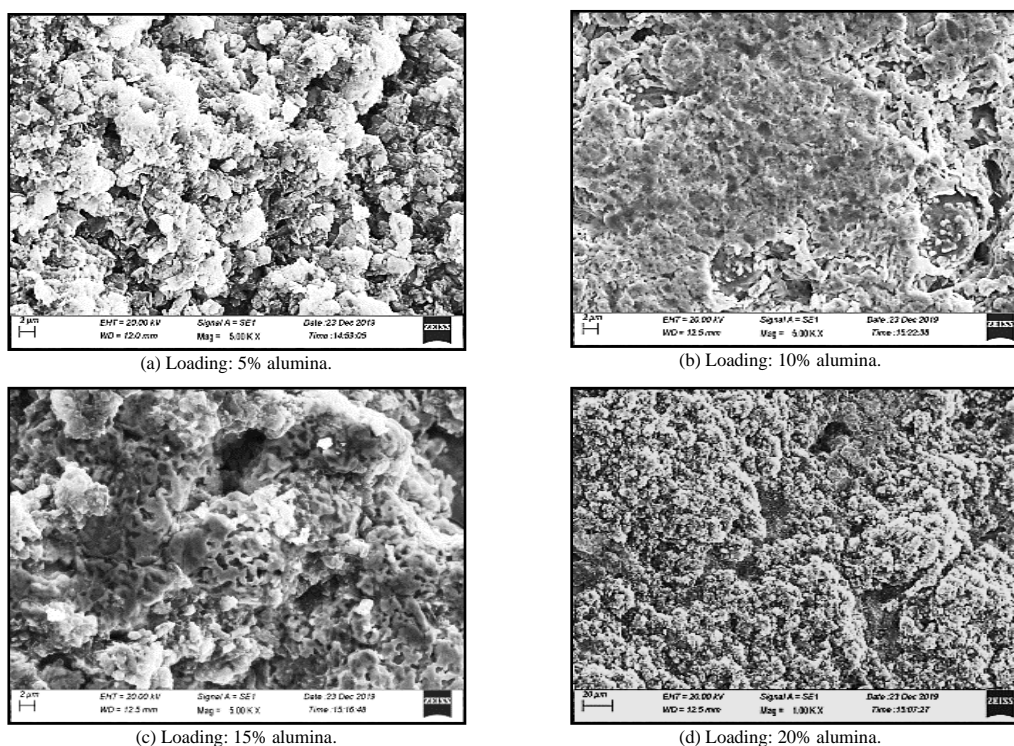
Adhesion of alumina-coated PSS tube sintered up to 700 °C.

Slurry no.	Solid loading of slurry (wt.%)	Weight of sample (gm)				Adhesion (%)
		Before coating (W _{initial})	After coating	After Sintering	After ultra-sonication (W _{final})	
1	5	10.884	10.937	10.962	10.927	0.4
2	10	8.429	8.536	8.602	8.533	1.2
3	15	7.758	8.231	8.068	7.900	1.8
4	20	7.627	8.117	7.892	7.763	1.8

Table 4

Gas permeation study of alumina coated PSS support.

Pressure (bar)	Flux (mol.m ⁻² .h ⁻¹)		Permeance (mol.m ⁻² .h ⁻¹ .Pa ⁻¹)		Gas selectivity (He/Ar)
	He	Ar	He	Ar	
0.05	120.84 ± 17	24.56 ± 10	0.024168	4.912 × 10 ⁻³	4.92
0.1	248.18 ± 17	61.03 ± 26	0.024818	6.103 × 10 ⁻³	4.06

**Fig. 8.** SEM images of alumina-coated PSS support with different solid loadings.

3.4 Studies on Pd-Cu membrane

3.4.1 Characterization of Pd-Cu membrane

The SEM and EDS analyses were carried out for unexposed, exposed, and regenerated Pd-Cu membranes. Fig. 9(a) shows that the unexposed membrane has a dense Pd-Cu layer. The EDS analysis of the unexposed membrane indicates the presence of Pd, Cu, Al, Si, and O (Fig. 9(b)). Fig. 9(c) shows the SEM image of the exposed membrane. It can be observed that sulfide formation has changed the morphology of the surface with patch-like dense structures. The presence of sulfur on the membrane surface was detected through EDS analysis (Fig. 9(d)). For 24 hours of exposure to the simulated gas environment, it was observed that sulfur covered the metal surface significantly. The SEM and EDS images (Fig. 9(e) - 9(h)) of the regenerated membrane show that sulfur was removed from the membrane surface by regeneration in the presence of an H₂ atmosphere, wherein the adsorbed sulfur possibly combines with H₂ and gets desorbed from the surface [51]. Fig. 9(i) cross-sectional morphology of unexposed membrane. The active metal layer thickness was around ~ 4 μm.

The XRD analysis results of unexposed Pd-Cu, exposed Pd-Cu, and Pd-Cu regenerated at 250 °C are shown in Fig. 10. The XRD peaks in unexposed Pd-Cu metal membrane correspond to the individual phases of Pd and Cu metal. However, peaks corresponding to Pd-Cu alloy were also observed in the case of exposed and regenerated membranes. After exposure to the simulated gas environment, peaks corresponding to Cu₂S and Pd₁₆S₇ on the metal surfaces were observed. However, the peaks corresponding to the sulfide of Pd-Cu alloy were not detected, which shows the stability of Pd-Cu in the sulfur environment. The presence of sulfur is also evident from EDS analysis results. In the XRD analysis of the regenerated membrane, the peaks corresponding to sulfides of Pd, Cu, and Pd-Cu were not detected, confirming the regeneration of the membrane.

Fig. 11 shows the membrane end connectors and permeator shell after exposure to a simulated biofuel environment. It can be observed that the end connectors have undergone corrosion as clearly evident by the change of color and deposition in some regions (portions encircled in red in Fig. 11). Inside the permeator shell, a crust-like deposition can also be seen, which is due to the formation of sulfides.

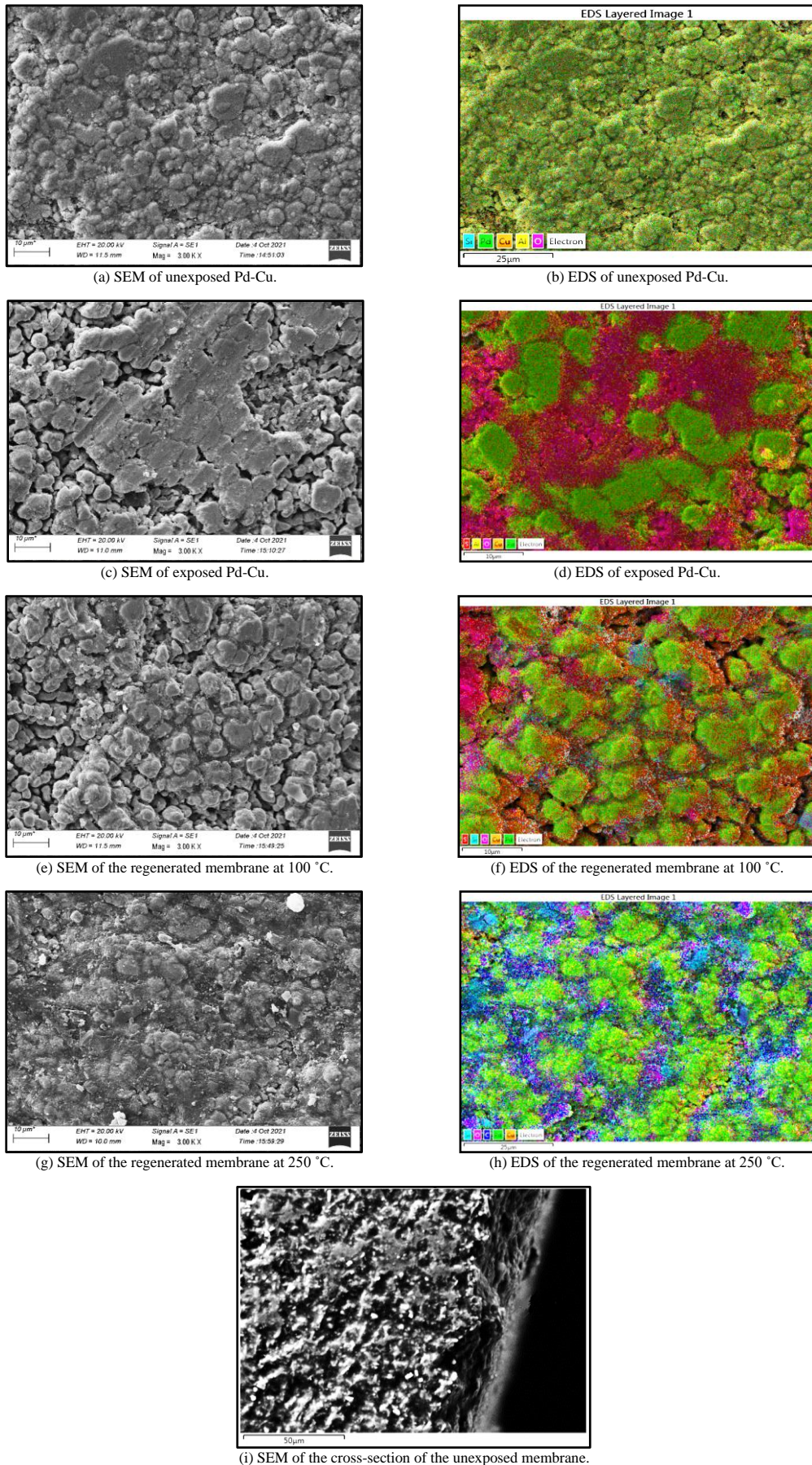


Fig.9. SEM and EDS images of exposed, unexposed, and regenerated Pd-Cu membrane.

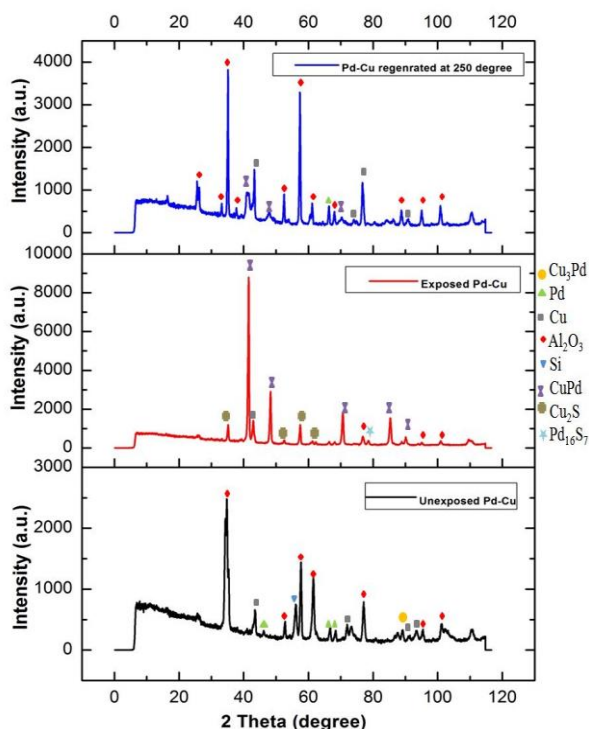


Fig. 10. The XRD patterns of unexposed, exposed, and regenerated Pd-Cu membrane at 250 °C.

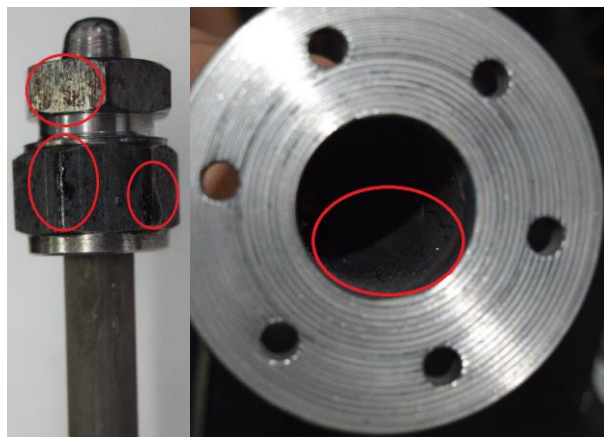


Fig. 11. Membrane end connectors and permeator shell after exposure to biofuel environment.

3.4.2 Gas permeation studies of unexposed membrane

Pd-Cu membrane was tested for gas permeation at 1 bar with hydrogen gas in batch mode for 185 minutes, and the hydrogen flow rate was found to be ~ 0.85 ml/min (permeance ~ 1 GPU). Experiments were carried out for hydrogen separation from a simulated stream having a composition similar to that of a vent stream in the biofuel production unit, at 1.5 and 2 bar for 280 minutes. The composition of the reject stream was analyzed at the end of the experiments. It was found that at 1.5 bar hydrogen concentration in the reject stream after 280 minutes was 52%, while at 2 bar it was 45%. Hence, a hydrogen recovery of 37% and 54% was achieved at 1.5 and 2 bar, respectively.

3.4.3 Gas permeation studies of exposed membrane

A gas permeation study of the exposed membrane (exposure duration of 24 hours) was carried out with hydrogen at 1 bar in batch mode for 105 minutes. The hydrogen flow rate was found to be ~ 0.22 ml/min (permeance ~ 0.25 GPU), which is approximately 25% of the initial flow. Since the membrane was exposed to a biofuel environment, hydrogen permeance was reduced. It is because of the formation of sulfides (Cu_2S and Pd_{16}S_7) on the membrane surface [34,37,52]. The XRD analysis also confirmed the presence of Cu_2S and

Pd_{16}S_7 phases after exposure to biofuel. Another reason for permeance reduction is the adsorption of CO and CO_2 on the membrane surface. As CO has a strong affinity toward the membrane surface, it tends to get adsorbed on the surface which further blocks the hydrogen adsorption sites, leading to a reduction in permeance [45,53]. The effective surface area for hydrogen dissociation gets reduced due to the presence of CO and CO_2 . The EDS analysis also confirmed the presence of carbon on the membrane.

3.4.4 Regeneration of exposed membrane

The membrane flux was reduced by 75% after exposure of 24 hours to a biofuel environment. Hence, the membrane was regenerated with H_2 (10%) - He (90%) gas mixture at 0.2 bar and temperatures of 100 and 250 °C for 5 hours. The flow rates of hydrogen at 100 and 250 °C were found to be 0.65 and 0.72 ml/min, respectively. During regeneration of membrane in a hydrogen-helium environment, the adsorbed sulfur tends to combine with H_2 and gets desorbed from the surface in the form of H_2S [29,36,51]. This leads to an increase in the average flow rate of hydrogen. The EDS analysis also confirmed that sulfur was removed from the membrane surface after regeneration of the membrane.

4. Conclusion

A composite Pd-Cu alloy membrane was developed to recover hydrogen from the hydrocracker's vent gas stream for recycling and reuse in the bio-jet fuel production unit. The membrane was developed by coating a thin film of Pd-Cu alloy over PSS support. The PSS support tubes were characterized by gas permeation studies and SEM analysis. The SEM analysis showed that the PSS has a pore size in the range of 5-10 μm and porosity was found to be ~ 20%. Gas permeation studies of the PSS support were carried out with helium and argon at different pressures (0.05 bar and 0.1 bar Pa). It was observed that the selectivity of PSS support for helium with respect to argon remained almost constant at 1.8 as pressure increased from 0.05 to 0.1 bar. In order to reduce the pore size of support, which is necessary to obtain a defect-free and thin coating of metal alloy on the support, an intermediate alumina layer was coated over the PSS using vacuum-assisted dip coating of support in alumina slurry with optimized composition (15% solid loading). The He/Ar selectivity of composite (PSS - alumina) support was found to increase in comparison to the bare PSS tube. A dense thin film (~ 4 microns) of Pd-Cu alloy was coated on the composite support using the DC magnetron sputter deposition technique. The performance of the composite palladium alloy membrane was evaluated with a simulated vent gas stream of the hydrocracker in the bio-jet fuel production unit. The initial membrane permeance was found to be ~ 1 GPU with a hydrogen recovery of 37 and 54% at 1.5 and 2 bar, respectively. The membrane permeance after exposure to a simulated environment for 24 hours was found to reduce by 75%. The membrane was regenerated by H_2 (10%) - He (90%) mixture at 0.2 bar and temperatures of 100 °C and 250 °C for 5 hours. At 250 °C, the flux was restored to up to 85% of the flux of the unexposed membrane. The work reported here has opened up newer possibilities for the application of metal membranes in the domain of bio-jet fuel production environment.

Acknowledgment

The authors are thankful to Mr. R. B. Bramhane, Mr. P. P. Surve, and Mr. A. K. Singha from Desalination and Membrane Technology Division, BARC; Dr. K. Singh from Material Science Division, BARC; Dr. L. Muhmood and Mr. G. V. Jawale from K. J. Somaiya College of Engineering, Mumbai for their valuable contribution in this work.

References

- [1] H. Wei, W. Liu, X. Chen, Q. Yang, J. Li, H. Chen, Renewable bio-jet fuel production for aviation: A review, *Fuel*. 254 (2019) 115599. <https://doi.org/10.1016/j.fuel.2019.06.007>
- [2] G. Bernardo, T. Araújo, T. da Silva Lopes, J. Sousa, A. Mendes, Recent advances in membrane technologies for hydrogen purification, *Int. J. Hydrogen Energy*. 45 (2020) 7313–7338. <https://doi.org/10.1016/j.ijhydene.2019.06.162>
- [3] I. IATA, International Air Transport Association, *Annu. Rev.* 2017 (2017). <https://www.iata.org/contentassets/c81222d96c9a4e0bb4ff6ced0126f0bb/iata-annual-review-2017.pdf>
- [4] F.B. Juangsa, L.A. Prananto, Z. Mufrodi, A. Budiman, T. Oda, M. Aziz, Highly energy-efficient combination of dehydrogenation of

- methylcyclohexane and hydrogen-based power generation, *Appl. Energy*. 226 (2018) 31–38. <https://doi.org/10.1016/j.apenergy.2018.05.110>
- [5] I.-H. Choi, K.-R. Hwang, J.-S. Han, K.-H. Lee, J.S. Yun, J.-S. Lee, The direct production of jet-fuel from non-edible oil in a single-step process, *Fuel*. 158 (2015) 98–104. <https://doi.org/10.1016/j.fuel.2015.05.020>
- [6] C. Gutiérrez-Antonio, A.G. Romero-Izquierdo, F.I. Gómez-Castro, S. Hernández, A. Briones-Ramírez, Simultaneous energy integration and intensification of the hydrotreating process to produce biojet fuel from *Jatropha curcas*, *Chem. Eng. Process. Process Intensif.* 110 (2016) 134–145. <https://doi.org/10.1016/j.cep.2016.10.007>
- [7] R.E.H. Sims, W. Mabee, J.N. Saddler, M. Taylor, An overview of second generation biofuel technologies, *Bioresour. Technol.* 101 (2010) 1570–1580. <https://doi.org/10.1016/j.biortech.2009.11.046>
- [8] M. Aziz, Integrated supercritical water gasification and a combined cycle for microalgal utilization, *Energy Convers. Manag.* 91 (2015) 140–148. <https://doi.org/10.1016/j.enconman.2014.12.012>
- [9] L. Yang, X. Ge, C. Wan, F. Yu, Y. Li, Progress and perspectives in converting biogas to transportation fuels, *Renew. Sustain. Energy Rev.* 40 (2014) 1133–1152. <https://doi.org/10.1016/j.rser.2014.08.008>
- [10] W. Guo, G. Li, Y. Zheng, S. Wang, Simulation study of thermochemical process from biomass to higher alcohols, *Energy & Fuels*. 30 (2016) 9440–9450. <https://doi.org/10.1021/acs.energyfuels.6b01687>
- [11] P. Li, K. Sakuragi, H. Makino, Extraction techniques in sustainable biofuel production: A concise review, *Fuel Process. Technol.* 193 (2019) 295–303. <https://doi.org/10.1016/j.fuproc.2019.05.009>
- [12] E. Martínez-Hernández, L.F. Ramírez-Verdusco, M.A. Amezcua-Allieri, J. Aburto, Process simulation and techno-economic analysis of bio-jet fuel and green diesel production—Minimum selling prices, *Chem. Eng. Res. Des.* 146 (2019) 60–70. <https://doi.org/10.1016/j.cherd.2019.03.042>
- [13] G. Liu, B. Yan, G. Chen, Technical review on jet fuel production, *Renew. Sustain. Energy Rev.* 25 (2013) 59–70. <https://doi.org/10.1016/j.rser.2013.03.025>
- [14] Y. She, S.C. Emerson, N.J. Magdefrau, S.M. Opalka, C. Thibaud-Erkey, T.H. Vanderspurt, Hydrogen permeability of sulfur tolerant Pd–Cu alloy membranes, *J. Membr. Sci.* 452 (2014) 203–211. <https://doi.org/10.1016/j.memsci.2013.09.025>
- [15] H. Yin, A.C.K. Yip, A review on the production and purification of biomass-derived hydrogen using emerging membrane technologies, *Catalysts*. 7 (2017) 297. <https://doi.org/10.3390/catal7100297>
- [16] W.-C. Wang, Techno-economic analysis of a bio-refinery process for producing Hydro-processed Renewable Jet fuel from *Jatropha*, *Renew. Energy*. 95 (2016) 63–73. <https://doi.org/10.1016/j.renene.2016.03.107>
- [17] M.C. Vasquez, E.E. Silva, E.F. Castillo, Hydrotreatment of vegetable oils: A review of the technologies and its developments for jet biofuel production, *Biomass and Bioenergy*, 105 (2017) 197–206. <https://doi.org/10.1016/j.biombioe.2017.07.008>
- [18] B.C. Nailwal, N. Goswami, R.K. Lenka, A.K. Singha, H.Z. Fani, A.S. Rao, A. Ghosh, R.C. Bindal, S. Mohan, S. Kar, Multi-tube tantalum membrane reactor for Hlx processing section of IS thermochemical process, *Int. J. Hydrogen Energy*, 45 (2020) 24341–24354. <https://doi.org/10.1016/j.ijhydene.2020.06.263>
- [19] N.W. Ockwig, T.M. Nenoff, Membranes for Hydrogen Separation, *Chem. Rev.* 107 (2007) 4078–4110. <https://doi.org/10.1021/cr0501792>
- [20] L. Wei, J. Yu, Y. Huang, Silver coating on porous stainless steel substrate and preparation of H₂-permeable palladium membranes, *Int. J. Hydrogen Energy*. 38 (2013) 10833–10838. <https://doi.org/10.1016/j.ijhydene.2013.02.137>
- [21] A. Li, J. R. Grace, C.J. Lim, Preparation of thin Pd-based composite membrane on planar metallic substrate. Part I: Pre-treatment of porous stainless steel substrate, *J. Membr. Sci.* 298 (2007) 175–181. <https://doi.org/10.1016/j.memsci.2007.04.016>
- [22] J.A. Medrano, E. Fernandez, J. Melendez, M. Parco, D.A.P. Tanaka, M. van Sint Annaland, F. Gallucci, Pd-based metallic supported membranes: High-temperature stability and fluidized bed reactor testing, *Int. J. Hydrogen Energy*. 41 (2016) 8706–8718. <https://doi.org/10.1016/j.memsci.2007.04.016>
- [23] Ø. Hatlevik, S.K. Gade, M.K. Keeling, P.M. Thoen, A.P. Davidson, J.D. Way, Palladium and palladium alloy membranes for hydrogen separation and production: History, fabrication strategies, and current performance, *Sep. Purif. Technol.* 73 (2010) 59–64. <https://doi.org/10.1016/j.seppur.2009.10.020>
- [24] Y.-H. Chi, P.-S. Yen, M.-S. Jeng, S.-T. Ko, T.-C. Lee, Preparation of thin Pd membrane on porous stainless steel tubes modified by a two-step method, *Int. J. Hydrogen Energy*. 35 (2010) 6303–6310. <https://doi.org/10.1016/j.ijhydene.2010.03.066>
- [25] S. Yun, S.T. Oyama, Correlations in palladium membranes for hydrogen separation: A review, *J. Membr. Sci.* 375 (2011) 28–45. <https://doi.org/10.1016/j.memsci.2011.03.057>
- [26] L. Wei, J. Yu, X. Hu, Y. Huang, Facile surface modification of porous stainless steel substrate with TiO₂ intermediate layer for fabrication of H₂-permeable composite palladium membranes, *Sep. Sci. Technol.* 51 (2016) 998–1006. <https://doi.org/10.1080/01496395.2015.1136330>
- [27] D. Wang, J. Tong, H. Xu, Y. Matsumura, Preparation of palladium membrane over porous stainless steel tube modified with zirconium oxide, *Catal. Today*. 93 (2004) 689–693. <https://doi.org/10.1016/j.cattod.2004.06.060>
- [28] D. Alique, M. Imperatore, R. Sanz, J.A. Calles, M.G. Baschetti, Hydrogen permeation in composite Pd-membranes prepared by conventional electroless plating and electroless pore-plating alternatives over ceramic and metallic supports, *Int. J. Hydrogen Energy*. 41 (2016) 19430–19438. <https://doi.org/10.1016/j.ijhydene.2016.06.128>
- [29] D. Alique, D. Martínez-Díaz, R. Sanz, J.A. Calles, Review of supported Pd-based membranes preparation by electroless plating for ultra-pure hydrogen production, *Membranes (Basel)*. 8 (2018) 5. <https://doi.org/10.3390/membranes8010005>
- [30] H. Klette, R. Bredesen, Sputtering of very thin palladium-alloy hydrogen separation membranes, *Membr. Technol.* 2005 (2005) 7–9. https://www.academia.edu/28574703/Sputtering_of_very_thin_palladium_alloy_hydrogen_separation_membranes?from=cover_page
- [31] T.A. Peters, M. Stange, R. Bredesen, Fabrication of palladium-based membranes by magnetron sputtering, *Palladium Membr. Technol. Hydrog. Prod. Carbon Capture Other Appl. Princ. Energy Prod. Other Appl.* (2014) 1–383. <https://doi.org/10.1533/9781782422419.1.25>
- [32] J.-Y. Han, C.-H. Kim, S.-H. Kim, D.-W. Kim, Development of Pd alloy hydrogen separation membranes with dense/porous hybrid structure for high hydrogen perm-selectivity, *Adv. Mater. Sci. Eng.* 2014 (2014). <https://doi.org/10.1155/2014/438216>
- [33] P.M. Thoen, F. Roa, J.D. Way, High flux palladium–copper composite membranes for hydrogen separations, *Desalination*. 193 (2006) 224–229. <https://doi.org/10.1016/j.desal.2005.09.025>
- [34] G.A.O. Huiyuan, W. Ling, Analysis of H₂S Tolerance of Pd–Cu Alloy Hydrogen Separation Membranes, *Chinese J. Chem. Eng.* 22 (2014) 503–508. [https://doi.org/10.1016/S1004-9541\(14\)60069-0](https://doi.org/10.1016/S1004-9541(14)60069-0)
- [35] B.H. Howard, R.P. Killmeyer, K.S. Rothenberger, A. V Cugini, B.D. Morreale, R.M. Enick, F. Bustamante, Hydrogen permeance of palladium–copper alloy membranes over a wide range of temperatures and pressures, *J. Membr. Sci.* 241 (2004) 207–218. <https://doi.org/10.1016/j.memsci.2004.04.031>
- [36] N. Pomerantz, Y.H. Ma, Effect of H₂S on the performance and long-term stability of Pd/Cu membranes, *Ind. Eng. Chem. Res.* 48 (2009) 4030–4039. <https://doi.org/10.1021/ie801947a>
- [37] J. Gabitto, C. Tsouris, Modeling sulfur poisoning of palladium membranes used for hydrogen separation, *Int. J. Chem. Eng.* 2019 (2019). <https://doi.org/10.1155/2019/9825280>
- [38] B.D. Morreale, M. V Ciocco, B.H. Howard, R.P. Killmeyer, A. V Cugini, R.M. Enick, Effect of hydrogen-sulfide on the hydrogen permeance of palladium–copper alloys at elevated temperatures, *J. Membr. Sci.* 241 (2004) 219–224. <https://doi.org/10.1016/j.memsci.2004.04.033>
- [39] N.A. Al-Mufachi, N. V Rees, R. Steinberger-Wilkens, Hydrogen selective membranes: A review of palladium-based dense metal membranes, *Renew. Sustain. Energy Rev.* 47 (2015) 540–551. <https://doi.org/10.1016/j.rser.2015.03.026>
- [40] H.T. Hoang, H.D. Tong, F.C. Gielen, H. V Jansen, M.C. Elwenspoek, Fabrication and characterization of dual sputtered Pd–Cu alloy films for hydrogen separation membranes, *Mater. Lett.* 58 (2004) 525–528. [https://doi.org/10.1016/S0167-577X\(03\)00539-1](https://doi.org/10.1016/S0167-577X(03)00539-1)
- [41] D.L. Mckinley, Metal alloy for hydrogen separation and purification, US Patent 3350845 (1967). <https://patentimages.storage.googleapis.com/83/d0/82/fc6159a6af242/U3350845.pdf>
- [42] D. Edlund, A membrane reactor for H₂S decomposition, USDOE Morgantown Energy Technology Center (METC), WV (United States), 1996. <https://www.osti.gov/servlets/purl/419404>
- [43] D.J. Edlund, A catalytic membrane reactor for facilitating the water-gas shift reaction at high temperature, Bend Research, Inc., OR (United States), 1994. http://fisher-tropsch.org/DOE/DOE_reports/9406131_22/edlund%20doe-er-81229-94-c0371.pdf
- [44] J.J. Conde, M. Marañón, J.M. Sánchez-Hervás, Pd-Based Membranes for Hydrogen Separation: Review of Alloying Elements and Their Influence on Membrane Properties, *Sep. Purif. Rev.* 46 (2017) 152–177. <https://doi.org/10.1080/15422119.2016.1212379>
- [45] K. Kian, C.M. Woodall, J. Wilcox, S. Liguori, Performance of Pd-based

- membranes and effects of various gas mixtures on H₂ permeation, *Environments*. 5 (2018) 128. <https://doi.org/10.3390/environments5120128>
- [46] S.H. Jung, K. Kusakabe, S. Morooka, S.-D. Kim, Effects of co-existing hydrocarbons on hydrogen permeation through a palladium membrane, *J. Membr. Sci.* 170 (2000) 53–60. [https://doi.org/10.1016/S0376-7388\(99\)00357-9](https://doi.org/10.1016/S0376-7388(99)00357-9)
- [47] O.U. Iyoha, Hydrogen production in palladium and palladium-copper membrane reactors at 1173K in the presence of hydrogen sulfide, (2007). <https://www.proquest.com/openview/e3575f2dd3fb1e8b341d9d26e77054b2/1?pq-origsite=gscholar&cbl=18750>
- [48] T. Yoshioka, E. Nakanishi, T. Tsuru, M. Asaeda, Experimental studies of gas permeation through microporous silica membranes, *AIChE J.* 47 (2001) 2052–2063. <https://doi.org/10.1002/aic.690470916>
- [49] E. Yalamaç, A. Trapani, S. Akkurt, Sintering and microstructural investigation of gamma–alpha alumina powders, *Eng. Sci. Technol. an Int. J.* 17 (2014) 2–7. <https://doi.org/10.1016/j.jestch.2014.02.001>
- [50] S.R. Chauruka, A. Hassanpour, R. Brydson, K.J. Roberts, M. Ghadiri, H. Stitt, Effect of mill type on the size reduction and phase transformation of gamma alumina, *Chem. Eng. Sci.* 134 (2015) 774–783. <https://doi.org/10.1016/j.ces.2015.06.004>
- [51] A. Kulprathipanja, G.O. Alptekin, J.L. Falconer, J.D. Way, Pd and Pd–Cu membranes: inhibition of H₂ permeation by H₂S, *J. Membr. Sci.* 254 (2005) 49–62. <https://doi.org/10.1016/j.memsci.2004.11.031>
- [52] B.D. Morreale, The influence of hydrogen sulfide on palladium and palladium-copper alloy membranes, *Diss. Abstr. Int.* 68 (2006). <http://d-scholarship.pitt.edu/9234/1/MorrealeBryan092006.pdf>
- [53] H. Gao, Y.S. Lin, Y. Li, B. Zhang, Chemical stability and its improvement of palladium-based metallic membranes, *Ind. Eng. Chem. Res.* 43 (2004) 6920–6930. <https://doi.org/10.1021/ie049722f>